Wall Cooling Effects on Hypersonic Transitional/Turbulent Boundary Layers at High Reynolds Numbers

Ralph D. Watson*
NASA Langley Research Center, Hampton, Va.

The characteristics of a thick hypersonic boundary layer that is turbulent for a length of 175 cm on a 4° sharp wedge have been measured. The resulting boundary layer was free from transverse curvature effects and only mildly affected by upstream history effects caused by pressure and wall temperature gradients. Heat-transfer distributions were used to locate regions of laminar, transitional, and turbulent flow at an edge unit Reynolds number of 0.47×10^6/cm at wall-to-total temperature ratios from about 0.3 to 1. Wall cooling had little effect on the location of the transition region. Pitot and total temperature profiles and skin-friction measurements also were obtained at several locations along the longitudinal centerline of the model. Mixing length and turbulent Prandtl number distributions were derived from the fully turbulent mean profiles.

Nomenclature

c_f = local skin-friction coefficient
c = specific heat
F_T = $(T_t - T_w)/(T_{t,e} - T_w)$
l = mixing length
M = Mach number
N = exponent in Eq. (5)
p = pressure
Pr = Prandtl number
q = static heat-transfer rate
R = Reynolds number
T = temperature
u = velocity
$\tilde{u}$ = generalized velocity = $\int_0^u (\rho/\rho_w)^{1/2}\,du$
u_τ = shear velocity = $(\tau_w/\rho_w)^{1/2}$
x,y = coordinates along and normal to body surface
y^+ = the quantity yu_τ/ν_w
δ = boundary-layer thickness
δ^* = displacement thickness
δ_I^* = $\int_0^\delta (1-u/u_e)\,dy$
δ^+ = the quantity $\delta u_\tau/\nu_w$
θ = momentum thickness
μ = molecular viscosity
ν = kinematic viscosity
ρ = density
τ = shear stress

Subscripts

e = edge value
L = laminar value
max = maximum value
p = pitot value
t = total value
T = turbulent value
v = based on velocity
w = wall value
∞ = freestream value

Presented as Paper 75-834 at the AIAA 8th Fluid and Plasma Dynamics Conference, Hartford, Conn. June 16-18, 1975; submitted July 19, 1976; revision received May 26, 1977.

Index category: Boundary Layers and Convective Heat Transfer – Turbulent.

*Aerospace Engineer, Applied Fluid Mechanics Section, High-Speed Aerodynamics Division. Member AIAA.

Introduction

In flat-plate boundary layers, a region exists in which the boundary layer is statistically turbulent but not yet in equilibrium. The term "equilibrium" here describes a turbulent boundary layer where the turbulence production and dissipation terms nearly balance, and similarity is maintained in the outer (wake-like) portion of the velocity profile.[1] This equilibrium flow sometimes will be referred to as a high Reynolds number flow, in contrast to the low Reynolds number region between the end of transition and equilibrium turbulent flow. Coles has discussed the low Reynolds number region of incompressible turbulent boundary layers in Ref. 2; other authors[3-6] have shown that quantities such as the mixing-length and turbulent Prandtl number distributions, which appear to be nearly invariant functions of y/δ at high Reynolds numbers, may differ considerably from the high Reynolds number description in this region. With increasing edge Mach number, the onset of transition is delayed, and the extents of both the transition region and low Reynolds number region grow. Thus, in hypersonic flow, it becomes important to be able to predict the characteristics of the transitional and low Reynolds number turbulent boundary-layer regions.

Boundary-layer calculations by finite-difference programs often are made using the mean field closure approach[7] for two reasons: mean field closure methods are relatively simple to set up, use, and modify, as compared to the more complicated higher-order closure methods; in addition, they are known to be accurate in many cases of practical interest.[8] Calculations are made by relating the turbulent shear to the mean velocity field and the turbulent heat conductivity to the mean temperature and velocity fields. For example, the finite-difference method of Ref. 9, used in this report for comparisons with data, uses a mixing-length approach to relate turbulent shear stress to the velocity field and a turbulent Prandtl number to relate the temperature field to the velocity field. Obviously, accurate predictions of skin friction and surface heating depend on accurate distributions of mixing-length and turbulent Prandtl number.

In hypersonic flow, turbulent boundary layers are strongly influenced by low Reynolds number effects. As shown in Ref. 10, heat transfer, skin friction, and velocity profile measurements at Mach 10 adiabatic wall conditions could not be predicted by finite-difference calculations using classical mixing-length constants. Better predictions of skin friction and velocity profiles were obtained by using variations of mixing-length parameters with Reynolds number.[11] However,

heat-transfer data were predicted poorly using currently available models of turbulent Prandtl number distributions.

The objective of this study is to provide accurate experimental test cases to validate prediction methods for calculating two-dimensional turbulent flow at high Mach number and high length Reynolds numbers. The test cases can be used to evaluate various turbulence models for the effects of compressibility and low Reynolds number for extreme flow conditions (Mach 10, $0.3 < T_w/T_t < 1$, and $\delta^+ < 700$). In addition to mean flow profiles, heat-transfer distributions, and skin-friction measurements, the turbulence parameters l/δ and Pr_T were derived from the profile data assuming local similarity.[3,12] It was found that when the thermal and velocity boundary-layer thicknesses differ significantly, as for the present data, the assumption of local similarity can lead to erroneous results in certain calculated quantities. A method is presented for insuring that the quantities calculated assuming local similarity are in agreement with the basic profile data.

Experimental Apparatus and Test Conditions

Tests were run in the Mach 20 leg of the High Reynolds Number Helium Tunnels described in Ref. 13. The nozzle is contoured and axisymmetric, and the test section and usable test core diameters are 152.4 and 50.8 cm, respectively. Total temperature is near ambient with an initial peak due to the tunnel starting process, and a subsequent constant decrease due to the bleed-down of the reservoir helium at fixed volume.

Most data were taken at a stagnation pressure of 1.38×10^4 kPa at nominal values of T_w/T_t of 0.3, 0.5, and 0.9. Test conditions for the majority of data to be presented are:

$$T_t = 311K, \quad T_w/T_t = 0.34\text{-}0.99, \quad M_\infty = 18.05$$

$$M_e = 10.9\text{-}11.8, \; R_e/m = 47 \times 10^6\text{-}59 \times 10^6 \; (33 \le \delta^+ \le 629)$$

Figure 1 is a sketch of the model, a 61×229-cm 4° wedge, having a sharp leading edge (0.1-mm maximum thickness) and top surface finish of 0.8 μ, rms. The model contained two chambers along the centerline which were instrumented with thermocouples, pressure orifices (0.23-cm i.d.), and skin-friction gages. For cold wall runs, the model was cooled with liquid nitrogen.

End plates extended to the height of the calculated inviscid shock to insure two-dimensional flow over the surface. Oil flow tests at near-adiabatic wall conditions showed that the flow was two-dimensional over most of the plate for the range of freestream test conditions covered in the investigation.

Surface heating rates were measured by the thin-skin technique at 73 locations along the model. The thermocouple plates were machined to a skin thickness of 0.051 cm for a diameter of 2.54 cm, and 30-gage iron-constantan thermocouples were spot-welded to the underside of the thin surface. Thermocouple conduction errors were insignificant, and the error in measured heating rates due to nonuniform surface temperature caused by the thin skin was calculated to be about 0.7%.

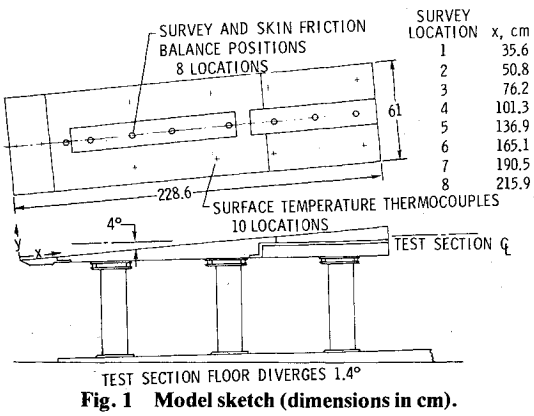

Fig. 1 Model sketch (dimensions in cm).

Pitot surveys were made with an axisymmetric probe having a tip diameter of 0.51 mm, as shown in Fig. 2. Total temperature surveys were made with a shielded, coiled-wire probe (essentially a resistance thermometer), which is described in Ref. 14. The total temperature at the edge of the boundary layer at the same x location as the survey probe was measured with a similar probe of larger dimensions. The temperature probe was constructed of 0.01-mm-diam coiled tungsten wire with a length-to-diameter ratio of approximately 800, which eliminated end loss corrections.

Pitot and total temperature probes were mounted on a hydraulic survey mechanism. The run time of the tunnel was 5 sec, of which 4 sec were available for data acquisition. Because of the relatively short run time, pitot and total temperature probes were stepped through the boundary layer rapidly, but with sufficient time for settling out of pressure and temperature. In addition to the physical lag of the measurement systems, time lag was introduced by the data recording system. The overall accuracy with which measured quantities could be correlated with y position was checked by performing reruns in certain cases. Repeatability was excellent, and errors in measured T_t and pitot pressure are estimated to be 2% at most.

Wall temperature at the survey locations was measured using a flattened iron-constantan thermocouple bonded to the surface approximately 2.5 cm to the side of and 2.5 cm behind the location at which the survey was made. Skin friction was measured with floating element balances manufactured by the Kistler Instrument Co. (model 322). Since the balances were required to operate in a vacuum and at cryogenic temperature, the operation and calibration of several balances were checked in a vacuum chamber at a pressure of 670 Pa and near liquid nitrogen temperature. Two balances were found to be suitable for use at these conditions. After calibration, the balances were fitted carefully to cases that were fitted to the instrumentation chambers.

Discussion of Results

Boundary-Layer Edge Conditions

At the test conditions of this investigation, the model shock was curved near the leading edge, producing a shock layer with significant entropy gradients. The resulting y variation of pitot pressure made it difficult to define the boundary-layer edge near the leading edge of the model. Downstream of the leading edge, the entropy gradient decreased as the shock-induced vortical flow was entrained by the boundary layer. When a constant pitot pressure was approached outside the boundary layer, the pitot boundary-layer thickness δ_p could be well defined as the point where $p_p/p_{p,e} = 0.995$. For stations near the leading edge, the thickness was somewhat arbitrary. Based on the measured pitot pressure at δ_p and the measured wall static pressure, the local Mach number and Reynolds number per meter were calculated[15] and are listed in Table 1.

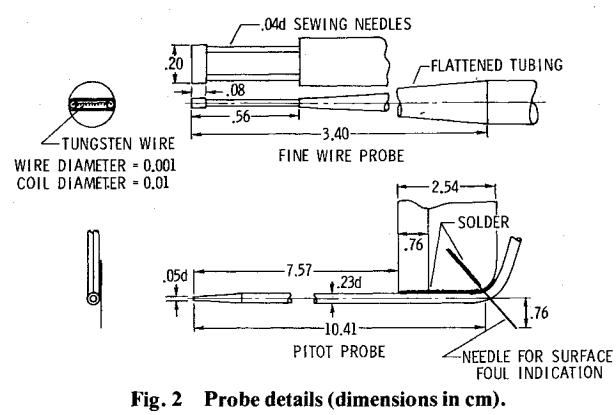

Fig. 2 Probe details (dimensions in cm).

Table 1 Mean flow boundary-layer properties and measured skin friction

Profile Data														Skin Friction Data		
Station	x, cm [a]	T_w/T_t	M_e	δ_p, cm	δ_v, cm	δ, cm	θ, cm	δ^*, cm	δ^+ [b]	N	R_θ	$R_{e,x}$	c_f inferred	c_f measured	T_w/T_t	$R_{e,x}$
1	35.6	.987	11.1	1.03	.62	---	4.7×10^{-3}	.54	33.3	---	2.32×10^3	2.11×10^7	1.501×10^{-4}	---	---	---
	35.6	.379	11.1	.90	.55	---	6.3	.46	70.8	---	3.22	2.19	.892	---	---	---
	35.6	.534	10.9	.90	.58	---	7.7	.43	---	---	3.73	1.73	---	---	---	---
2	50.5	.948	11.2	1.27	.90	---	8.2	.76	45.4	---	3.77	2.32	1.477	1.477×10^{-4}	.93	2.05×10^7
	50.5	.429	11.3	1.14	.66	---	7.0	.49	87.5	---	3.32	2.40	1.600	1.584	.36	2.01
	50.5	.557	11.3	1.27	.74	---	7.3	.58	79.8	---	3.63	2.49	1.200	1.812	.49	2.10
3	75.9	.946	11.0	1.91	1.00	---	10.9	.74	80.6	---	5.21	3.62	3.521	3.075	.93	3.18
	75.9	.521	11.1	1.78	.97	---	10.0	.79	196.6	---	5.15	3.92	3.400	4.600	.40	3.43
	75.9	.588	11.2	2.03	.99	---	9.9	.81	151.8	---	5.37	4.11	3.186	3.362	.49	3.52
4	101.3	.933	11.0	2.40	1.44	---	1.6×10^{-2}	1.18	123.0	---	8.33	5.23	3.126	2.993	.94	4.64
	101.3	.370	10.9	1.80	1.17	---	1.9	.85	317.6	---	9.49	5.13	4.134	3.622	.35	4.43
	101.3	.468	10.9	2.00	1.18	---	1.3	.96	241.7	---	6.78	5.18	4.101	3.439	.49	4.53
5	136.9	.935	11.1	2.96	1.74	2.03	1.9	1.49	144.4	10.	1.01×10^4	7.15	2.990	2.834	.92	5.31
	136.9	.400	11.2	2.50	1.79	1.96	2.6	1.15	405.8	11.	1.35	7.24	3.563	3.036	.34	5.91
	136.9	.508	11.2	2.82	1.66	2.03	2.1	1.30	291.1	11.	1.09	7.27	3.457	3.695	.47	6.02
6	165.1	.925	11.2	3.18	2.46	2.12	2.1	1.73	188.0	12.	1.10	8.78	2.700	2.542	.90	7.23
	165.1	.387	11.2	2.74	1.98	2.12	2.6	1.39	445.3	11.	1.38	8.65	3.400	2.819	.33	7.15
	165.1	.488	11.2	2.67	1.93	2.12	2.5	1.46	328.9	10.	1.30	8.88	3.000	2.785	.48	7.48
7	190.5	.957	11.4	4.00	2.39	3.39	2.6	2.18	173.2	9.	1.43	1.06×10^8	2.453	2.326	.92	8.88
	190.5	.392	11.5	3.50	1.98	2.54	2.5	1.68	428.2	10.	1.36	1.04	3.300	2.801	.37	9.34
	190.5	.473	11.5	4.00	2.39	2.54	2.4	1.96	397.6	10.	1.29	1.04	2.812	2.528	.50	9.51
8	215.9	.950	11.6	4.57	2.70	2.99	2.8	2.39	190.3	9.	1.61	1.25	2.259	2.134	.92	1.04×10^8
	215.9	.343	11.5	3.63	2.67	2.42	3.1	1.80	629.4	10.	1.63	1.15	3.200	2.561	.31	1.03
	215.9	.463	11.8	3.94	2.81	2.82	3.0	2.05	462.7	10.	1.80	1.30	2.650	2.303	.47	1.16
	215.9	---	---	---	---	---	---	---	---	---	---	---	---	1.82	.92	1.56
	215.9	---	---	---	---	---	---	---	---	---	---	---	---	2.17	.35	1.52

[a] Listed values of x for pitot surveys; station 5 c_f measurements at $x = 131.2$. [b] Based on δ_v and c_f measured except at station 1.

Extent of the Transition Region

Heat-transfer measurements were used to locate regions of laminar, transitional, and turbulent flow. The location of transition was little affected by wall cooling at constant freestream unit Reynolds number, in agreement with the results of Ref. 16; however, changing the freestream unit Reynolds number caused corresponding changes in the transition location. Transition Reynolds numbers exhibit an approximate 0.4 power-law variation with the freestream unit Reynolds number. Examples of measured heating rates presented in Fig. 3 show that, for a Reynolds number of 0.47×10^6/cm and two T_w/T_t values, the location of the transition region is little changed by variation of T_w/T_t. Also shown are data at a Reynolds number of 0.25×10^6/cm, which demonstrate the change in the transition location with unit Reynolds number.

Measured pressures on the model surface further demonstrate the small variation of the transition location with wall cooling. Figure 4 shows the pressure distributions and displacement thickness measurements at hot and cold wall conditions. For comparison, δ^* from a finite-difference boundary-layer calculation[9] at $T_w/T_t = 0.33$ is also shown. Near the beginning of transition, δ^* decreases due to a rapid filling-out of the velocity profile, with the result that the external flow expands and the surface pressure decreases. As δ^* resumes its normal growth, the expanded edge flow is compressed increasing the surface pressure. The location of peak surface pressure does not change for the range of T_w/T_t investigated; however, the peak pressure occurs downstream of peak heating (see Fig. 3).

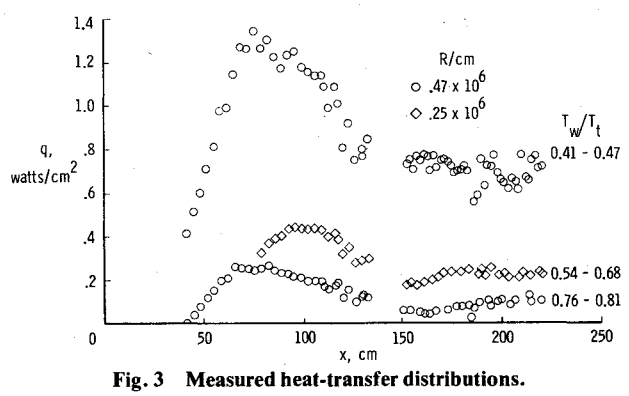

Fig. 3 Measured heat-transfer distributions.

Pitot and Total Temperature Surveys

In order to calculate mean velocity and density profiles at each station, pitot pressure surveys were combined with total

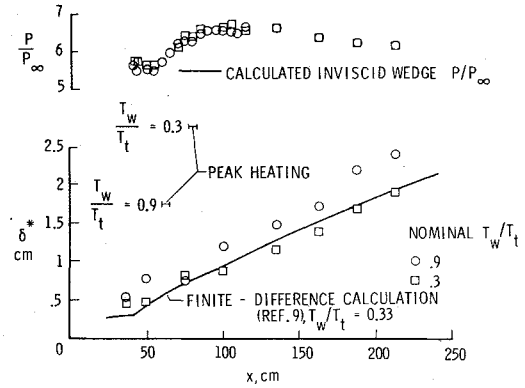

Fig. 4 Surface pressures and displacement thicknesses at $R/\text{cm} = 0.47 \times 10^6$.

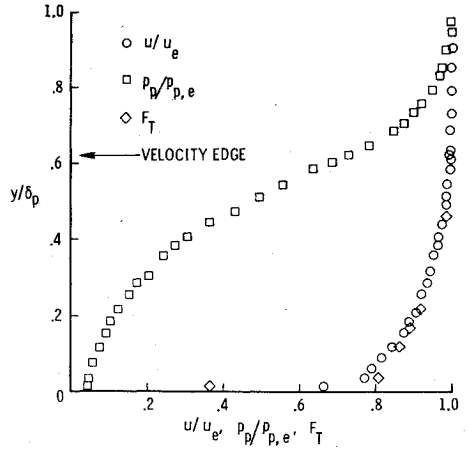

Fig. 5 Representative velocity, pitot, and total temperature profiles at $T_w/T_t = 0.39$.

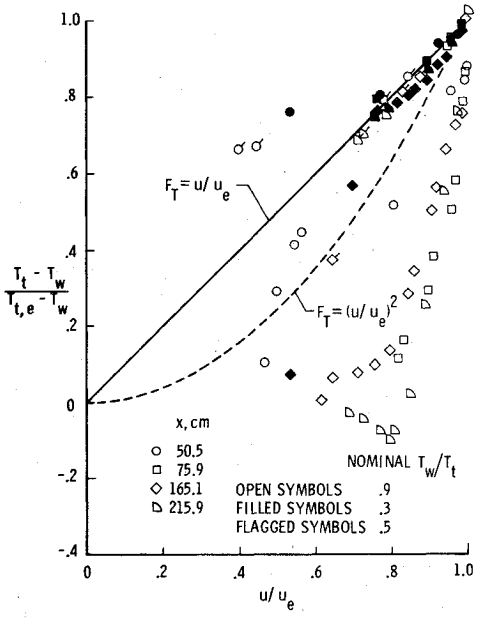

Fig. 6 Total temperature profiles in Crocco form.

temperature surveys and measured surface pressures. Since neither the tunnel total temperature nor the model temperature could be accurately preset, variations of T_w/T_t occurred from run to run. In order to combine total temperature surveys with pitot surveys at slightly different values of T_w/T_t, total temperatures were reduced to the Crocco parameter $(T_t - T_w)/(T_{t,e} - T_w)$, using measured instantaneous values of T_w and $T_{t,e}$. The values of $T_{t,e}$ and T_w at the end of the 4 sec total temperature survey were taken to be representative of the combined pitot-total temperature data, even though the pitot data may have been measured at a slightly different value of T_w/T_t. These values are listed in Table 1 for a total of 24 cases at 8 survey locations and 3 values of T_w/T_t.

Representative velocity, temperature, and pitot profiles are shown in Fig. 5. The thermal boundary-layer thickness, which closely corresponds to the pitot boundary-layer thickness, is 50-60% greater than the velocity boundary-layer thickness $(u/u_e = 0.995)$ for the cases shown. Flat-plate or nozzle-wall total temperature profiles in Crocco coordinates are usually well-behaved for cold wall conditions, approximating either a linear or quadratic relation of the form

$$(T_t - T_w)/(T_{t,e} - T_w) = u/u_e \quad \text{or} \quad (u/u_e)^2 \qquad (1)$$

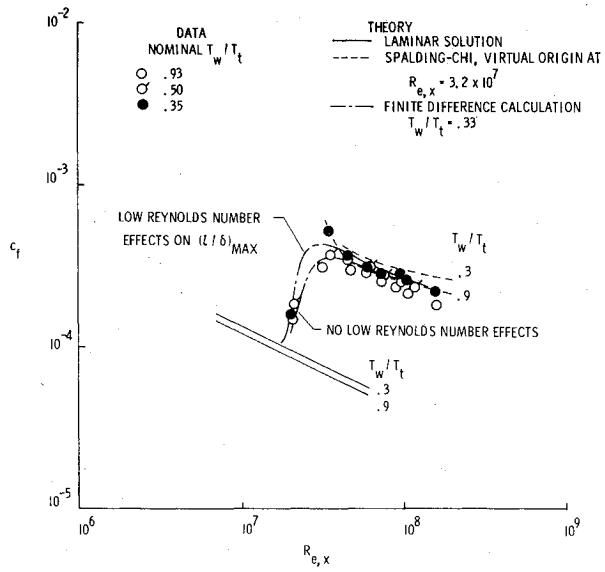

Fig. 7 Skin-friction data.

In high-speed turbulent flow at near-adiabatic wall conditions, experimental temperature profiles show a marked deviation from Eq. (1). Examples of the present data, shown in Fig. 6, exhibit trends similar to those of Refs. 10 and 17 at hot wall conditions; however, the cold wall cases more nearly follow the linear relation usually found for flat-plate data.[18] The reason for this behavior at hot wall conditions is not known at the present time. From Eq. (1) it is evident that, as T_w approaches $T_{t,e}$, experimental errors are magnified in Crocco coordinates. For example, for T_t typical of the present tests, a 1% error in $T_t/T_{t,e}$ measurement results in a 25% error in F_T at $T_w/T_t = 0.96$. The measurement error of the present T_w/T_t data, estimated to be less than 2%, could not explain the trends shown in the data of Fig. 7. The departure from Eq. (1) at hot wall conditions occurs at least as early as 76 cm (near peak heating), and persists without significant change for about 30 boundary-layer thicknesses.

Skin-Friction Measurements

Direct measurements of skin friction were made at seven model centerline stations corresponding to survey stations 2 through 8. Because of the physical constraints imposed by the mounting arrangement, measurements could not be made at station 1; also, station 5 was 5.7 cm upstream of the corresponding survey position. Measured skin-friction coefficients based on local flow conditions are listed in Table 1. Included in the table are data at station 8 for a Reynolds number per meter of 7.1×10^9; in reducing the data to coefficient form, the Mach number at station 8 was assumed to be the same as that for a R_e/m of 4.8×10^9.

The data are presented in Fig. 7 and are compared with predictions by three different methods. Zero pressure gradient skin friction was calculated for laminar flow by a similar solution (method of Ref. 19), and for turbulent flow by Spalding and Chi's method,[20] using a virtual origin at 80% of the peak heating location, as recommended in Ref. 21. Both laminar and turbulent values are shown for $T_w/T_t = 0.3$ and 0.9. Also shown are c_f values for two finite-difference calculations at $T_w/T_t = 0.33$, using 0.4 for the slope of the mixing length at the wall and 26 for the wall damping constant.[3] In one case $(l/\delta)_{max}$ was held fixed at 0.08; in the other case the variation of $(l/\delta)_{max}$ with δ^+ from Ref. 11 was used. The Spalding-Chi prediction is approximately 20% higher than the data at both hot and cold wall conditions. The finite-difference calculation, which includes low Reynolds number effects on $(l/\delta)_{max}$, agrees well with the data, except near the peak value of skin friction.

Reduced Velocity Profiles

It often is difficult to measure surface shear directly, and usually inaccurate to calculate it from the slope of the velocity profile at the wall. Thus, it would be invaluable to be able to estimate skin friction accurately from the law-of-the-wall region velocity profiles, away from the laminar sublayer where probe interference effects may be present. Reference 22 showed that, by using generalized velocities $\tilde{u}$,[23,24] compressible profiles were reduced to incompressible profiles in law-of-the-wall form for isoenergetic flows at Mach numbers as high as 3.78. In Ref. 10, the technique worked well in hypersonic helium flow for nearly isoenergetic flow ($T_w/T_t \simeq 1$), and skin friction obtained by trial-and-error fitting of the velocity profile to the incompressible law-of-the-wall agreed well with measured values. Reference 25 showed that cold wall velocity profiles in air at Mach numbers as high as 7.4 can be reduced adequately using $\tilde{u}$, and that skin-friction values agree "reasonably well" with directly measured values.

The present velocity profile data have been reduced using generalized velocities and a trial-and-error procedure to find u_τ for each profile. Skin friction is obtained from u_τ by the relation

$$c_f/2 \equiv \rho_w/\rho_e\,(u_\tau/u_e)^2 \tag{2}$$

The following equation is used for the incompressible law-of-the-wall:

$$\begin{aligned} u/u_\tau &= y^+ \quad \text{in sublayer} \\ &= (1/0.43)\ \ln y^+ + 5.1 \text{ in logarithmic region} \end{aligned} \tag{3}$$

The constants 0.43 and 5.1 in Eq. (3) accurately represent reduced hypersonic helium data.[10] Representative cold wall generalized velocity profiles obtained from experimental mean velocity profiles are shown in Fig. 8. The compressible profiles are satisfactorily reduced to the incompressible relation, Eq. (3), for stations downstream of transition. Skin-friction values obtained by this method are listed in Table 1, along with measured values of c_f. The density profiles necessary to define $\tilde{u}$ were calculated using measured total temperature distributions.

At hot wall conditions, the error in inferred skin friction is nowhere greater than 6% of the measured value, at intermediate wall temperatures the average error is 11%, and at cold wall conditions the average error is 20%. Thus, this method of inferring skin friction from velocity profiles appears to be accurate only near adiabatic wall conditions. In fully turbulent flow, inferred skin-friction values always are higher than measured (balance) values for the present data.

Derived Profile Quantities

A previous study[10] of near-adiabatic wall hypersonic flat plate turbulent boundary layers has shown that accurate predictions of flow properties cannot be made in the boundary layer immediately following transition, the region of low Reynolds number effects. In order to better understand the reason for the discrepancy between experimental results and predictions by finite-difference calculations, mixing length and turbulent Prandtl number distributions, which are inputs to finite-difference calculation methods, were derived from the fully turbulent mean profiles of the present investigation at stations 5 to 8. The derivation of these quantities requires either sufficient data to define derivatives of the mean flow quantities in the streamwise direction or the assumption that the profiles are similar. For the present data, the four surveys in the fully turbulent region of the boundary layer were not sufficient to determine the streamwise derivatives accurately, so that the similarity assumption was necessary.

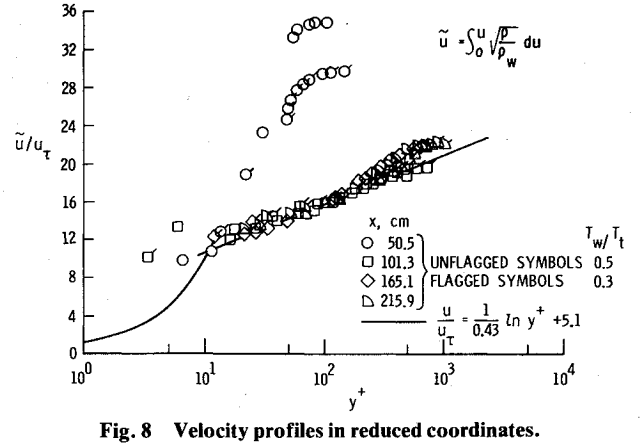

Fig. 8 Velocity profiles in reduced coordinates.

The local similarity equations of Refs. 3 and 12 were used to calculate the shear stress and energy flux through the boundary layer, and to obtain Pr_T and l from the calculated quantities. Isentropic flow at the edge of the boundary layer was used to relate dp/dx to mass flow and dynamic pressure gradient terms in the equations. The molecular viscosity was calculated by the following equation:

$$\mu = 5.023\,[T^{1.647}/(T+0.83)] \quad \text{(micropoise)} \quad \text{for } T \text{ in Kelvin} \tag{4}$$

This equation fits the helium data shown in Ref. 26 better at low temperatures than the 0.647 power-law relation, often used.

The application of the local similarity equations requires that u/u_e and $T_t/T_{t,e}$ be known functions of y/δ, and that δ and $d\delta/dx$ be known. For the present data, as for other data at high Mach numbers in helium,[10,27] the velocity edge δ_v and the pitot edge of the boundary layer δ_p do not coincide. Even at the most upstream survey station, the thicknesses differ (see Table 1), suggesting that the difference may be a feature of the initial laminar boundary layer. The flowfield near the leading edge contains two mechanisms that might produce differing thicknesses: the favorable pressure gradient (neglecting the immediate tip region), which persists until transition occurs; and vorticity in the shock layer, produced by the δ^* induced shock curvature.[28] Laminar similar solutions, using the equations of Ref. 19 and a 0.647 viscosity-temperature power law for helium, show that, at $M_e = 11$, $\delta_v/\delta_p = 0.91$-0.94 for $T_w/T_t = 0.3$-0.9, and, in general, as M_e increases, $\delta_v/\delta_p \to 1$. The effect of favorable pressure gradients on similar solutions was examined, and it was found that increasing the pressure gradient parameter[19] decreased slightly δ_v/δ_p; however, it could not account for the low ratios observed in the present data. The most probable cause of the difference in thicknesses is finite vorticity external to the boundary layer caused by viscous induced shock curvature. This has been suggested in Ref. 29 as the cause of a similar effect in the data of Fischer and Maddalon.[27]

When a difference between δ_v and δ_p occurs, neither thickness is a correct similarity parameter, since the total temperature, density, and velocity thicknesses do not coincide. That is, these quantities approach the limiting edge conditions at a different rate. For example, when the turbulence modeling parameters originally were derived from the present data using δ_p as the similarity thickness, the integral of the momentum loss through the boundary layer differed from the wall shear stress by a factor of 2[30]. Since the profiles are not truly similar, a suitably derived δ must be used to assure that the momentum and heat flux balances through the boundary layer are retained, and that calculated negative shear stress values do not appear in the outer region of the boundary layer. There can be two such thicknesses, one for shear stress, and one for heat flux. Only the shear stress thickness δ was considered here, although the same thickness produced reasonable matches in integrated heat fluxes with measured surface values, except for the hot wall cases.

The δ to be used in the similarity equations was taken to be the value of y beyond which a contribution to the integral value of the momentum thickness was insignificant. This point was found by plotting

$$\int \rho u/\rho_e u_e \left[1-(u/u_e)\right] dy/y$$

vs $1/y$. As y increases without limit, both the ordinate and abscissa approach zero. Initial deviation of the integrated quantity from a straight line through the origin, although somewhat arbitrary, was taken to denote δ. The resulting values, which lie in between the velocity and pitot thicknesses, are listed in Table 1. The slope, $d\delta/dx$, was found by plotting δ as a function of x, fairing a curve through the data, and finding the tangent to the curve at the desired location. The velocity thickness δ_v was found to exhibit less scatter than δ_p or δ, which were more sensitive to T_w/T_t. The slopes obtained by plotting any of the three thicknesses gave approximately the same results in the turbulent region.

In addition to the turbulence quantities, values of the power-law exponent N were calculated for each profile. The value of N is defined by the following equation:

$$u/u_e = (y/\delta_v)^{1/N} \tag{5}$$

Reference 30 shows that the power-law velocity profile is correctly scaled by δ_v rather than δ_p when there are significant differences in these two thicknesses. Values of N derived for the present data are listed in Table 1.

Examples of mixing-length distributions derived from similarity relations and mean profiles are compared in Fig. 9a, with the incompressible distribution ($k=0.4$, $(l/\delta)_{max}=0.09$). The mixing length scale and the y coordinate are nondimensionalized by δ_v. If δ_p had been used instead of δ_v, the shape of the mixing length distributions shown would not change; however, the values of l/δ would be well below the incompressible distribution. Significant increases in l/δ in the outer region of the boundary layer occur as δ^+ decreases. This trend is typical of flat-plate turbulent boundary layers, though not of nozzle wall boundary layers.[31] Other values of $(l/\delta)_{max}$ derived from mean flow profiles are compared with the present data and with the faired curve from Ref. 11 in Fig. 9b. The scatter in the data suggests that parameters other than δ^+ also might be necessary in correlating $(l/\delta)_{max}$.

Total shear stress profiles for the present data are shown in Fig. 10 along with a curve of the incompressible data of Ref. 32. The present results are higher than the incompressible results; however, they are in general agreement with the body of data presented in Ref. 33 which tend to lie on or slightly above the incompressible curve at higher values of y/δ. The derived similarity thickness δ has been used in plotting the present shear stress distributions.

Fairings of the turbulent Prandtl number distributions from the present data are shown in Fig. 11, along with experimental flat-plate data from Mach 2.5 to 4.5 from Ref. 6. All data are characterized by a peak near the wall, decaying to an almost constant value above a y^+ value of about 100 (i.e., probably in the wake region for the present profiles – see Fig. 8). No trend, either in the location of the peak value of Pr_T,

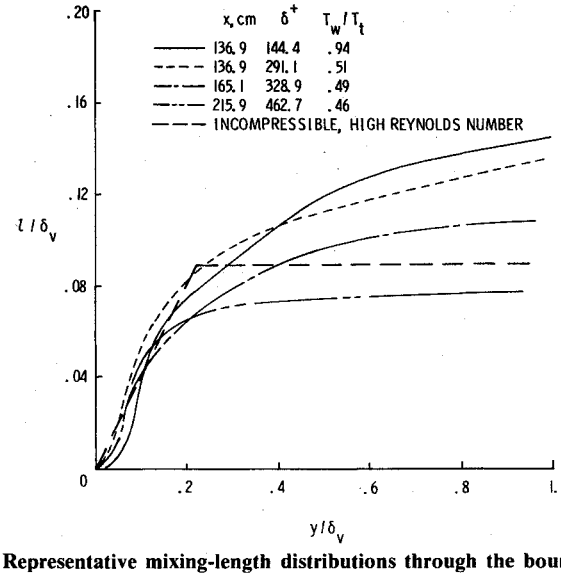

a) Representative mixing-length distributions through the boundary layer.

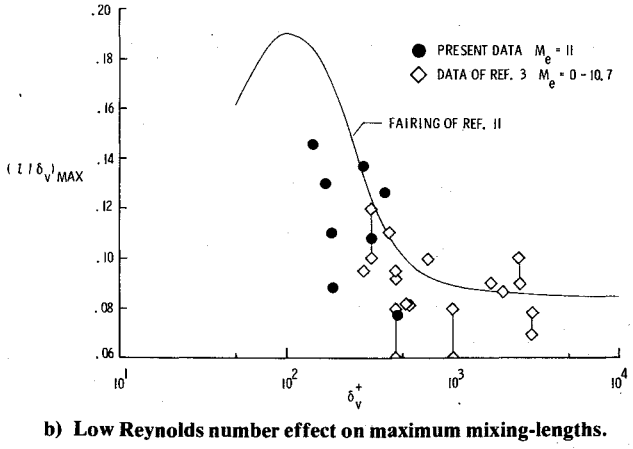

b) Low Reynolds number effect on maximum mixing-lengths.

Fig. 9 Turbulence parameters derived from mean profiles.

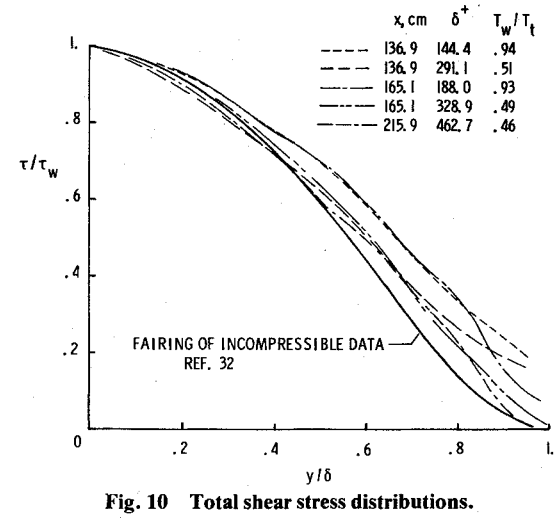

Fig. 10 Total shear stress distributions.

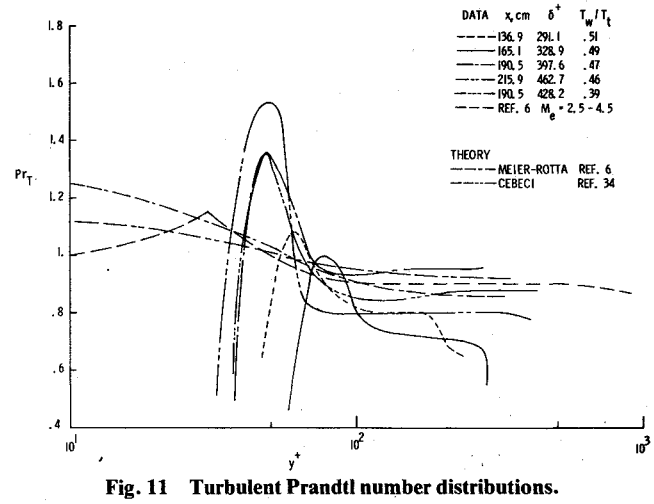

Fig. 11 Turbulent Prandtl number distributions.

the level of the peak, or the level in the outer region, is obvious from the data shown in Fig. 11. Theoretical predictions from Refs. 6 and 34, also shown in Fig. 11, continue to increase toward the wall. The accuracy of the experimental Pr_T distributions decrease with decreasing y^+ due to possible probe interference effects near the wall.

The present data cannot resolve the question of whether or not the turbulent Prandtl number actually decreases within the sublayer and buffer region. Finite-difference calculations made by the author (not shown herein) indicate that wall heat-transfer rates at $M_e = 11$ and $T_w/T_t = 0.9$ are strongly affected by the Prandtl number distributions near the wall, whereas at cold wall conditions they are not. Allowing the Pr_T to decrease near the wall results in better predictions of measured heating rates than does an increasing Pr_T with decreasing y^+ for the hot wall condition.

Concluding Remarks

Extensive measurements of the mean flow properties of hypersonic turbulent boundary layers at various wall-to-total temperature ratios have led to the following conclusions:

1) Skin-friction coefficients, inferred by fitting generalized experimental velocity profiles to the incompressible law-of-the-wall, are too high at cold wall conditions; the discrepancy decreases as T_w/T_t increases.

2) The value of l/δ, when scaled with the velocity thickness of the boundary layer, agrees with incompressible results better than if scaled with the thermal or pitot thickness.

3) Low Reynolds number effects in the present data follow the same trends found in previously obtained data; that is, there is an increase in the level of l/δ as δ^+ decreases.

4) The turbulent Prandtl number was found to increase as the interface between the laminar sublayer and the logarithmic velocity profile region is approached. This trend is in agreement with other flat-plate data. There is evidence that Pr_T decreases below values of y^+ of approximately 50; however, the correct trend cannot be ascertained accurately from the present data.

References

[1] Townsend, A.A., "Equilibrium Layers and Wall Turbulence," *Journal of Fluid Mechanics,* Vol. 11, 1961, pp. 97-120.

[2] Coles, D.E., "The Turbulent Boundary Layer in a Compressible Fluid," The Rand Corp., Rept. No. R-403-PR, 1962.

[3] Bushnell, D.M. and Morris, D.J., "Shear Stress, Eddy Viscosity, and Mixing Length Distribution in Hypersonic Turbulent Boundary Layers," NASA TM X-2310, Aug. 1971.

[4] Huffman, G.D. and Bradshaw, P., "A Note on von Karman's Constant in Low Reynolds Number Turbulent Flows," *Journal of Fluid Mechanics,* Vol. 53, Pt. 1, 1972, pp. 45-60.

[5] Cebeci, T., "Kinematic Eddy Viscosity at Low Reynolds Numbers," *AIAA Journal,* Vol. 11, Jan. 1973, pp. 102-104.

[6] Meier, H.E. and Rotta, J.C., "Temperature Distributions in Supersonic Turbulent Boundary Layers," *AIAA Journal,* Vol. 9, Nov. 1971, pp. 2149-2156.

[7] Bushnell, D.M., Cary, A.M., Jr., and Harris, J.E., "Calculation Methods for Compressible Turbulent Boundary Layers," *Lecture Notes for von Karman Institute for Fluid Dynamics* (AGARD) Lecture Series on Compressible Turbulent Boundary Layers, Rhode-St. Genese, Belgium, March 1-5, 1976.

[8] Beckwith, I.E., "Recent Advances in Research on Compressible Turbulent Boundary Layers," Paper No. 18 in Analytic Methods in Aircraft Aerodynamics, NASA SP-228, Oct. 28-30, 1969.

[9] Bushnell, D.M. and Beckwith, I.E., "Calculation of Nonequilibrium Hypersonic Turbulent Boundary Layers and Comparisons with Experimental Data," *AIAA Journal,* Vol. 8, Aug. 1970, pp. 1462-1469.

[10] Watson, R.D., Harris, J.E., and Anders, J.B., Jr., "Measurements in a Transitional/Turbulent Mach 10 Boundary Layer at High Reynolds Numbers," AIAA Paper 73-165, New York, Jan. 10-12, 1973.

[11] Bushnell, D.M. and Alston, D.W., "Calculation of Transitional Boundary Layer Flows," *AIAA Journal,* Vol. 11, April 1973, pp. 554-556.

[12] Horstman, C.C. and Owen, F.K., "Turbulent Properties of a Compressible Boundary Layer," *AIAA Journal,* Vol. 10, Nov. 1972, pp. 1418-1424.

[13] Watson, R.D. and Bushnell, D.M., "Calibration of the Langley Mach 20 High Reynolds Number Helium Tunnel Including Diffuser Measurements," NASA TM X-2353, Oct. 1971.

[14] Weinstein, L.M., "Hot-Wire Coil Probe for High Speed Flows," *AIAA Journal,* Vol. 11, Dec. 1973, pp. 1772-1773.

[15] Ames Research Staff: "Equations, Tables, and Charts for Compressible Flow," NACA Rept. 1135, 1953.

[16] Fischer, M.C., "Influence of Moderate Wall Cooling on Cone Transition at $M_e = 13.7$ in Helium," *Journal of Spacecraft and Rockets,* Vol. 10, April 1973, pp. 282-283.

[17] Mabey, D.G., Meier, H.U., and Sawyer, W.G., "Some Boundary Layer Measurements on a Flat Plate at Mach Numbers from 2.5 to 4.5," Paper presented at Fluid Dynamics Panel Specialists' Meeting, AGARD-CP-93, Sept. 13-15, 1971.

[18] Bushnell, D.M., Johnson, C.B., Harvey, W.D., and Feller, W.V., "Comparison of Prediction Methods and Studies of Relaxation in Hypersonic Turbulent Nozzle-Wall Boundary Layers," NASA TN D-5433, 1969.

[19] Beckwith, I.E. and Cohen, N.B., "Application of Similar Solutions to Calculation of Laminar Heat Transfer on Bodies with Yaw and Large Pressure Gradient in High-Speed Flow," NASA TN D-625, 1961.

[20] Spalding, D.B. and Chi, S.W., "The Drag of a Compressible Turbulent Boundary Layer on a Smooth Flat Plate With and Without Heat Transfer," *Journal of Fluid Mechanics,* Vol. 18, Pt. 1, Jan. 1964, pp. 117-143.

[21] Cary, A.M., Jr., "Summary of Available Information on Reynolds Analogy for Zero-Pressure-Gradient, Compressible, Turbulent-Boundary-Layer Flow," NASA TN D-5560, Jan. 1970.

[22] Mathews, D.C., Childs, M.E., and Paynter, G.D., "Use of Coles' Universal Wake Function for Compressible Turbulent Boundary Layers," *Journal of Aircraft,* Vol. 7, March-April 1970, pp. 137-140.

[23] van Driest, E.R., "Turbulent Boundary Layer in Compressible Fluids," *Journal of the Aeronautical Sciences,* Vol. 18, 1951, pp. 145-160, p. 216.

[24] Danberg, J.E., "A Re-evaluation of Zero Pressure Gradient Compressible Turbulent Boundary Layer Measurements," Paper presented at Fluid Dynamics Panel Specialists' Meeting, AGARD-CP-93, Sept. 13-15, 1971.

[25] Sun, C.C. and Childs, M.E., "A Wall-Wake Velocity Profile for Turbulent Compressible Boundary Layers with Heat Transfer," NASA-CR-119131, 1975.

[26] Maddalon, D.V. and Jackson, W.E., "A Survey of the Transport Properties of Helium at High Mach Number Wind-Tunnel Conditions," NASA TM X-2020, 1970.

[27] Fischer, M.C. and Maddalon, D.V., "Experimental Laminar, Transitional and Turbulent Boundary Layer Profiles on a Wedge at Local Mach Number 6.5 and Comparisons with Theory," NASA TN D-6462, 1971.

[28] Lewis, C.H., "Comparison of a First-Order Treatment of Higher-Order Boundary Layer Effects with Second-Order Theory and Experimental Data," AEDC-TR-68-148, Oct. 1968.

[29] Sullivan, P.A. and Koziak, W.W., "Entropy Layer Effects in Constant Pressure Hypersonic Boundary Layers," *AIAA Journal,* Vol. 11, May 1973, pp. 730-731.

[30] Watson, R.D., "Wall Cooling Effects on Transitional/Turbulent Boundary Layers at High Reynolds Numbers," Hartford, Conn., June 16-18, 1975.

[31] Bushnell, D.M., Cary, A.M., Jr., and Holley, B.B., "Mixing Length in Low Reynolds Number Compressible Turbulent Boundary Layers," *AIAA Journal,* Vol. 13, Aug. 1975, pp. 1119-1121.

[32] Tetervin, N., "A Semi-Empirical Derivation of Friction, Heat-Transfer, and Mass-Transfer Coefficients for the Constant Property Turbulent Boundary Layer on a Flat Plate," Naval Ordnance Lab., 63-77, AD-422359, Oct. 1963.

[33] Sandborn, V.A., "A Review of Turbulence Measurements in Compressible Flow," NASA TM X-62337, March 1974.

[34] Cebeci, T., "A Model for Eddy Conductivity and Turbulent Prandtl Number," *Journal of Heat Transfer,* Vol. 95, May 1973, pp. 227-234.